Self-Assembly of Tetramers of 5,6-Dihydroxyindole Explains the Primary Physical Properties of Eumelanin: Experiment, Simulation, and Design

Chun-Teh Chen,[†] Vincent Ball,[‡,§,⊥,∥] José Joaquim de Almeida Gracio,[¶,×] Manoj Kumar Singh,[¶,×] Valérie Toniazzo,[‡] David Ruch,[‡] and Markus J. Buehler[†,#,▲,*]

[†]Laboratory for Atomistic and Molecular Mechanics, Department of Civil and Environmental Engineering, Massachusetts Institute of Technology, 77 Massachusetts Avenue, Room 1-235A&B, Cambridge, Massachusetts 02139, United States, [‡]Department for Advanced Materials and Structures, Centre de Recherche Public Henri Tudor, 5 rue Bommel, L-4940 Hautcharage, Luxembourg, [§]Faculté de Chirurgie Dentaire, Université de Strasbourg, 1 Place de l'Hôpital, 67000 Strasbourg, France, [⊥]Institut National de la Santé et de la Recherche Médicale, UMR 1121, 11 rue Humann, 67085 Strasbourg Cédex, France, [∥]Fédération de Médecine Translationelle de Strasbourg, 1 Place de l'Hôpital, 67000 Strasbourg, France, [¶]Center for Mechanical Technology and Automation, Department of Mechanical Engineering, University of Aveiro, Campus Universitário Santiago, 3810-193 Aveiro, Portugal, [×]Aveiro Institute of Nanotechnology, University of Aveiro, 3810-193 Aveiro, Portugal, and [#]Center for Materials Science and Engineering and [▲]Center for Computational Engineering, Massachusetts Institute of Technology, 77 Massachusetts Avenue, Cambridge, Massachusetts 02139, United States

ABSTRACT Eumelanin is a ubiquitous pigment in nature and has many intriguing physicochemical properties, such as broad-band and monotonous absorption spectrum, antioxidant and free radical scavenging behavior, and strong nonradiative relaxation of photoexcited electronic states. These properties are highly related to its structural and mechanical properties and make eumelanin a fascinating candidate for the design of multifunctional nanomaterials. Here we report joint experimental—computational investigation of the structural and mechanical properties of eumelanin assemblies produced from dopamine, revealing that the mass density of dry eumelanin is 1.55 g/cm^3 and its Young's modulus is ≈5 GPa. We also find that wet eumelanin has a lower mass density and Young's modulus depending on the water-to-melanin ratio. Most importantly, our data show that eumelanin molecules tend to form secondary structures based on noncovalent π stacking in both dry and wet conditions, with an interlayer distance between eumelanin molecules of 3.3 Å. Corresponding transmission electron microscope images confirm the supramolecular organization predicted in our simulations. Our simulations show that eumelanin is an isotropic material at a larger scale when eumelanin molecules are randomly oriented to form secondary structures. These results are in good agreement with experimental observations, density functional theory calculations, and bridge the gap between earlier experimental and small-scale quantum mechanical studies of eumelanin. We use the knowledge acquired from the simulations to select a partner molecule, a cationic phthalocyanine, allowing us to produce layer-by-layer films containing eumelanin that display an electrical conductivity 5 orders of magnitudes higher than that of pure eumelanin films.

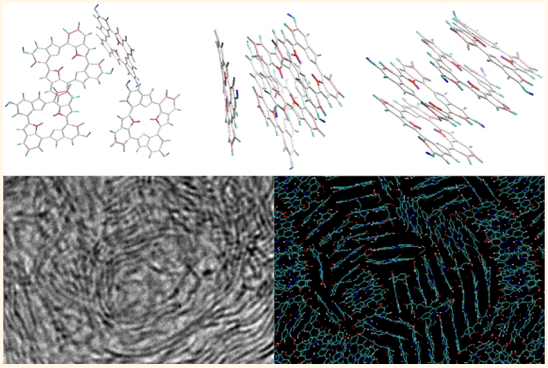

KEYWORDS: eumelanin · self-assembly · molecular dynamics · mechanical properties · electrical conductivity

Eumelanin is a ubiquitous pigment in nature and has many intriguing physicochemical properties: broad-band and monotonous absorption spectrum, antioxidant and free radical scavenging behavior, and strong nonradiative relaxation of photoexcited electronic states.[1] Multifunctional properties of eumelanin are highly related to its structural and mechanical properties (*e.g.*, the self-assembly mechanism and the size distribution of secondary structures) and have led to the suggestion that it could be useful as a biologically inspired material, particularly in the form of thin films.[2,3] The physicochemical properties of a single eumelanin molecule cannot

* Address correspondence to mbuehler@mit.edu.

Received for review November 15, 2012 and accepted January 15, 2013.

Published online January 15, 2013
10.1021/nn305305d

represent these properties of eumelanin. In order to have a better understanding of eumelanin's multifunctional properties, the knowledge of its structural and mechanical properties is mandatory. There are two distinct types of melanins in nature: the black-brown eumelanin and the yellow-reddish pheomelanin, which often coexist together in living organisms.[4] Eumelanin is a fascinating material owing to its bio-optoelectronic, its dielectric,[5] and metal chelating properties.[6] In addition, natural eumelanin can be isolated in large quantities from the ink sacs of the cuttlefish *Sepia officinalis* allowing *in vitro* studies using physical techniques.[7,8]

It is well-established that fundamental building blocks of eumelanin are 5,6-dihydroxyindolequinone (DHI) or hydroquinone (HQ), its redox forms indolequinone (IQ), tautomers quinone-methide (MQ), quinoneimine (NQ), and 5,6-dihydroxyindole-2-carboxylic acid (DHICA).[9] However, much less information is available about the further evolution of these building blocks to eumelanin. One of the major fundamental questions concerning melanins is their real chemical nature, which, for a long time, has been suspected to be a heterogeneous polymer and difficult to characterize owing to its insolubility in most organic solvents. However, the X-ray scattering experiments performed by Cheng *et al.*[10,11] as well as the scanning tunneling microscopy (STM) experiments performed by Zajac *et al.*,[12] suggested that eumelanin is a heterogeneous aggregate of stacked oligomers. More and more experimental evidence is in favor of the heterogeneous aggregate model[13,14] and suggests that the basic aggregate is made of not more than five or six IQ units. Recent nuclear magnetic resonance (NMR) experiments[15] as well as controlled degradation experiments showed that the average degree of polymerization in eumelanins is low.[16] In addition, matrix-assisted laser desorption−ionization mass spectrometry showed the presence of ions with *m*/*z* values not higher than 1500 in the mass spectra, consistent with the presence of small aggregates in eumelanin.[17] Although some experimental studies have proposed molecular structures and aggregate structures of eumelanin based on the experimental observations, they have not yet included any computational studies (*e.g.*, with molecular dynamics simulations) to test if the proposed eumelanin models can represent the properties of eumelanin. Despite a significant experimental and theoretical effort, the molecular structure of eumelanin remains controversial. Even though numerous theoretical calculations are available for IQ, the known precursor of eumelanin, and its small oligomers,[18,19] the gap between these aggregates and their assembly into eumelanin particles has not yet been fully bridged.

Recently, Kaxiras *et al.*[20] proposed a new, detailed structural model for eumelanin protomolecules, based on a tetrameric structure consisting of four monomer units, in arrangements that contain an inner porphyrin ring (Supporting Information Figure S1). In a further step, Meng and Karixas[21] performed density functional theory (DFT) calculations in order to establish a transition to higher level aggregates. They found that two such IMIM or HMHM tetramers can not only associate in a quasi-parallel arrangement with an interlayer distance of 3.0−3.3 Å through π stacking and van der Waals interactions but also bind in a covalent manner through interlayer C−C bonds. These investigators, however, restricted their system to only two tetramers (due to the limitations of DFT calculations) and hence cannot represent the properties of eumelanin. It is of the highest interest to enlarge the system to have more realistic information about the formation of eumelanin, which can reach apparent molecular masses of more than 10^7-10^9 g·mol^{-1} as inferred from static dynamic light scattering experiments.[22] This means that a eumelanin particle could contain between about 2×10^4 and 2×10^6 tetramers. It is not yet possible to perform simulations of the self-assembly of such large systems notwithstanding the fact that the hydration water of eumelanin should be taken into account. However, it is mandatory to go from the dimer of tetramers investigated by Meng and Kaxiras[21] to somewhat larger and realistic systems made of some hundreds of tetramers. In this paper, it is our aim to describe a model allowing us to predict most of the physical properties of eumelanin from molecular dynamics simulations, based on the self-assembly of the most stable tetramer of 5,6-dihydroxyindole, the IMIM porphyrin-like tetramer, whose energy was found to be the lowest among all possible tetramers of IQ.[20] In addition, the knowledge acquired from these simulations allows us to design a new composite of eumelanin displaying an increase in electrical conductivity by 5 orders of magnitude with respect to pure eumelanin films.

In this paper, we use the eumelanin model proposed by Kaxiras *et al.*[20,21] to study the self-assembly of eumelanin molecules of which we optimized the geometry and energy and compared the obtained simulated structure with the structure of synthetic eumelanin grains as characterized by means of high-resolution transmission electron microscopy (TEM). In addition, other properties such as the mass density and Young's modulus of the simulated structure are compared with available experimental data.

RESULTS AND DISCUSSION

In order to calculate the equilibrium distance of eumelanin molecules, we set up a simple system with only two IMIM tetramers, and the initial distance between these two IMIM tetramers is adjusted to be 1.8 Å. After energy minimization, the equilibrium distance is calculated to be 3.3 Å, which is very close to the experimental and DFT results.[21] To start the investigation of the self-assembly mechanism of eumelanin molecules, we set up another simple system with four

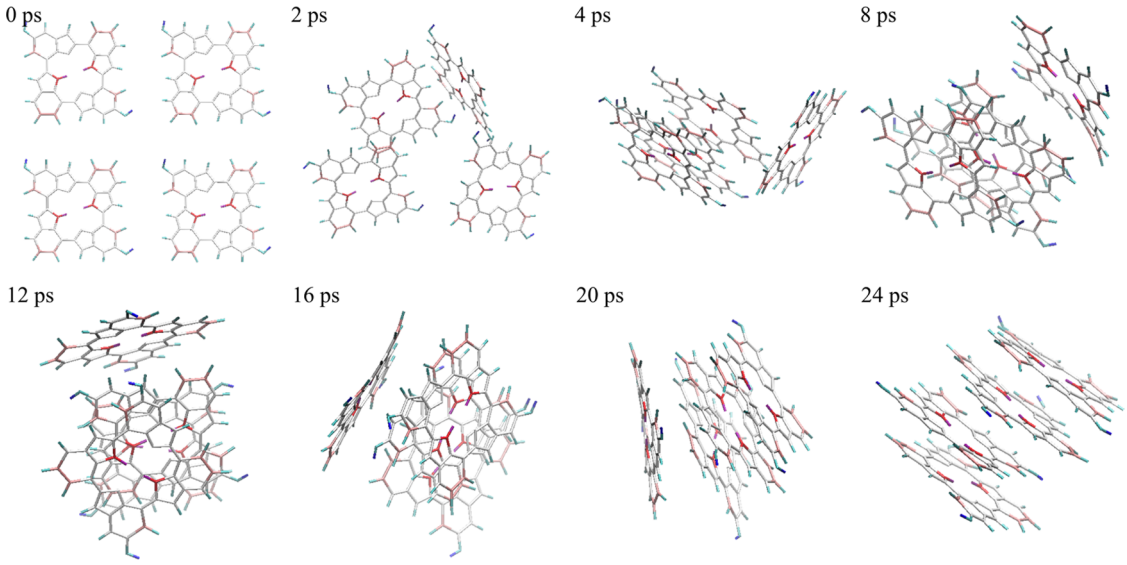

Figure 1. Snapshots of the self-assembly process of four IMIM tetramers. The four IMIM tetramers are separated from each other in the initial configuration but quickly stack together to form a secondary structure.

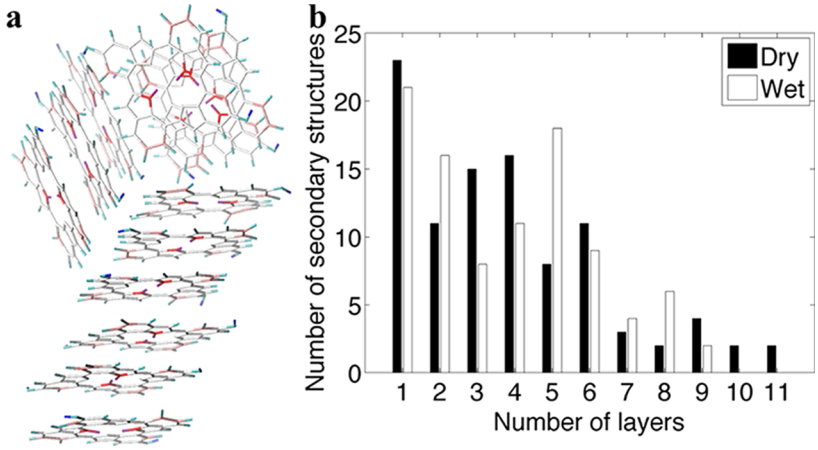

Figure 2. (a) Snapshot of the 12 IMIM tetramers at the steady state of self-assembly. There are three secondary structures: one of them contains six IMIM tetramers, and the other two both contain three IMIM tetramers. Hence, in this system, the average number of stacked layers is 4.0 since there are 12 IMIM tetramers in three secondary structures. (b) Distribution of the aggregate size obtained by analyzing the number of eumelanin molecules stacked in an aggregate made of 375 IMIM tetramers in the dry and wet eumelanin systems.

IMIM tetramers. After energy minimization, the system is simulated with the NPT ensemble at a constant temperature of 300 K, and the snapshots of the system are shown in Figure 1. These four IMIM tetramers are separated from each other in the initial configuration but stacking together to form a secondary structure after 24 ps.

We set up another system with 12 IMIM tetramers to study the size distribution of secondary structures of eumelanin. After energy minimization, the system is simulated with the NVT ensemble at a constant temperature of 300 K for 1.0 ns, and the snapshot of the system after 1.0 ns of simulation is shown in Figure 2a. We can see that there are three secondary structures: one of them contains six IMIM tetramers, and the other two both contain three IMIM tetramers. Hence, in this system, the average number of stacked layers is 4.0 since there are 12 IMIM tetramers in three secondary structures. These secondary structures are also attracting each other *via* van der Waals interactions to form an even larger structure. We then extended this investigation to our large-scale systems made of 375 IMIM tetramers. The distribution of the IMIM tetramers in stacked aggregates made of *n* molecules is given in Figure 2b for the dry and wet eumelanin systems. At the steady state of the simulation in the dry eumelanin system, there are only 23 IMIM tetramers among 375 (*i.e.*, 6.1%) not forming secondary structures. The criteria used to define if two IMIM tetramers are stacked together or not are detailed in the Modeling and Experimental Methods section. In the wet eumelanin system, made of the same number of IMIM tetramers,

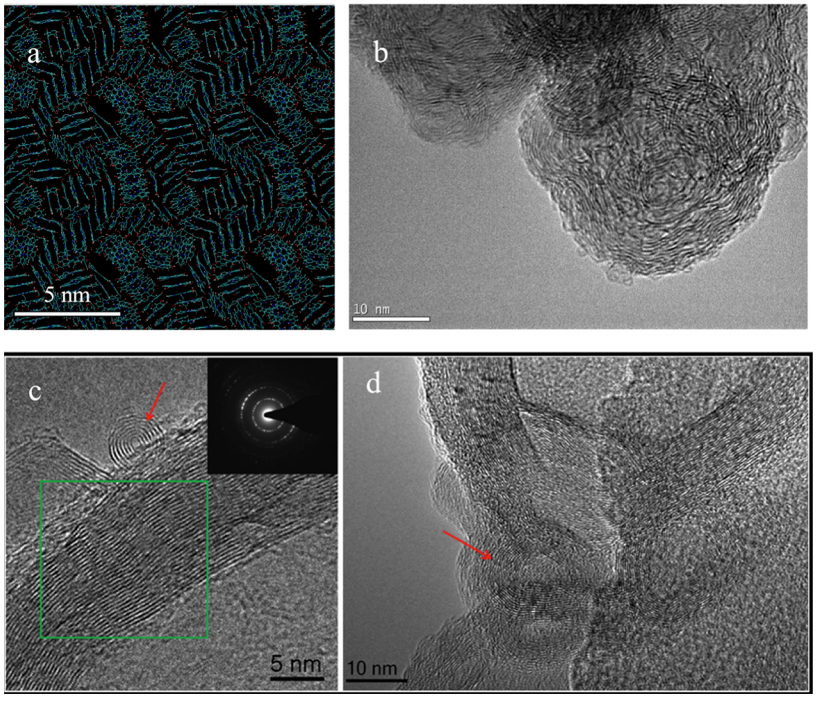

Figure 3. (a) Snapshot of the simulated aggregate made of 375 IMIM tetramers at the steady state of self-assembly. (b) Typical TEM micrograph of eumelanin produced from the oxidation of dopamine (2 g·L^{-1} in an aerated Tris buffer, at 50 mM and at pH 8.5, reaction time of 24 h). (c,d) High-resolution TEM images of eumelanin on other locations of the TEM grid. The inset of panel c shows a SAED pattern taken from the green-boxed region. The red arrow in panels c and d indicates that the molecules aggregate and form an onion-like nanostructure composed of stacked planes arranged in concentric rings.

there are only 21 IMIM tetramers (*i.e.*, 5.6%) not forming secondary structures. The average numbers of stacked layers are 3.87 and 3.95 in the dry and wet eumelanin systems, respectively. In addition, we also find that IMIM tetramers will less likely favor forming secondary structures at higher temperatures.

The *X*, *Y*, and *Z* components of the orientation vector of each IMIM tetramer in the dry and wet eumelanin systems are shown in Supporting Information Figure S2a,b, respectively. We can see that the orientations of eumelanin molecules are almost random in both dry and wet conditions. This means that there is no favorable orientation at long-range scale for eumelanin molecules. No matter what kind of initial configuration is chosen, we observe that IMIM tetramers tend to arrange themselves in random-like orientations. This suggests that the random-like arrangement of eumelanin molecules is more energetically favorable. The method used to define the orientation vector of each IMIM tetramer is detailed in the Modeling and Experimental Methods section.

The snapshot of the dry eumelanin system at the steady state is shown in Figure 3a. For clarity, we only show the IMIM tetramers that are in a 10 Å range of the *Z* direction. We can see that the snapshot reveals a simulated aggregate structure similar to those contained in synthetic eumelanin produced from an oxygenated dopamine solution (2 mg·mL^{-1} in an aerated Tris buffer, at 50 mM and at pH 8.5, the reaction time being 24 h) (Figure 3b). In both the simulated and experimentally obtained structure, some stacked aggregates are found, the distance between stacked eumelanin molecules being 3.3 Å on average, which is very close to the interlayer distance of graphite.[23] In addition, the self-assembly mechanism of eumelanin molecules also seems to be similar to graphene fragments.[24] The presence of ordered cylinders of aggregates randomly oriented through the cluster was also found in the TEM images produced by Meredith *et al.*[25] Our simulation results of the self-assembly of IMIM tetramers allow us to reproduce the experimentally observed structure of eumelanin grains (another TEM image is available in Supporting Information Figure S3) obtained from a dopamine solution in oxidizing conditions (pH 8.5 in an open reactor to allow for a permanent influx of O_2, which serves as an oxidant). In these conditions, dopamine undergoes a first oxidation to dopaquinone, followed by an intramolecular Michael addition to leucodopachrome, which oxidizes further in dopachrome to yield 5,6-dihydroxyindole[26] according to the classical Raper–Mason mechanism.[27] The grains obtained by this way display a ^{13}C solid-state NMR spectrum, which is indistinguishable from that of natural eumelanin.[28] The X-ray photoelectron spectroscopy (XPS) spectra of these grains are also compatible with the composition of eumelanin.[28]

We can hence reasonably assume that the grains displayed in Figure 3b are made of eumelanin. In addition to the similar aggregate structure, the mass density of eumelanin calculated from the *in silico* self-assembly of

IMIM tetramers is equal to 1.55 g/cm^3 for the dry eumelanin system and 1.38 g/cm^3 for the wet eumelanin system, and the results are in good agreement with experimental studies (Table 1).[13,29−31] The Young's modulus of eumelanin is calculated from the curves shown in Figure 4a,b for the dry and wet eumelanin systems, respectively, and is found to be 5.0 ± 1.7 GPa for the dry *in silico* eumelanin system and 2.3 ± 1.3 GPa for the corresponding wet eumelanin system. In addition, the stress−strain curves displayed in Figure 4a,b show that eumelanin is an isotropic material, in agreement with the random distribution of the aggregates (Supporting Information Figure S2). Note that studying only a few IMIM tetramers cannot capture the isotropic feature of eumelanin, and hence, eumelanin might show highly anisotropic behavior at a smaller scale. The comparison with the experimentally determined Young's modulus of eumelanins is given in Table 2.[30,32] Once again, the agreement between the *in silico* values and the experimental data is very good.

Our simulations show that making the assumption that the eumelanin molecule is a tetramer of IQ, the IMIM tetramer, which corresponds to the lowest energy of all possible tetramers of IQ,[20] is sufficient to predict *in silico* the properties of eumelanin. Hence, this work gives an additional proof of evidence that the "stacked oligomer" model allows us to explain the structural and mechanical properties of eumelanin. For the first time, to our knowledge, the gap between IQ and its small oligomers has been bridged to allow for the formation of eumelanin containing a reasonable number of tetramers (375). Our model suggests that the formation of huge aggregates of IQ is not mandatory for the self-assembly of eumelanin. Looking at simulated structures as those predicted *in silico* and observed experimentally (Figure 3b−d, Supporting Information Figure S3, see also ref 25), one understands why eumelanin should display a small electrical conductivity, even if the dispersion of the available experimental data is large probably due to noncontrolled hydration during the measurement: each domain of π stacked aggregates should have similar conductivity as graphite (the average interlayer distance obtained from the simulations is also close to 3.4 Å), but all of these domains are randomly connected. Knowing the structure of our *in silico* produced eumelanin model made of tetramers having the structure of porphyrins (Supporting Information Figure S1), we made the assumption that such structure should interact with cationic phthalocyanines, which are used as conductors in organic photovoltaics[33] and structurally close to porphyrins, to provide some improved electrical conductivity to eumelanin grains. The probability for strong interactions of eumelanin grains with the cationic Alcyan Blue (AB) (Supporting Information Figure S4) is high due not only to possible π stacking with eumelanin but also to electrostatic interactions, eumelanin being negatively charged at all pH values above 4.[34]

The interactions between AB and synthetic eumelanin were investigated by the deposition of films in a layer-by-layer manner[35] to build up (AB-melanin)$_n$ films. The absorbance of those films at the wavelengths corresponding to the Soret band (420 nm) and the Q bands of AB (650−800 nm) increases linearly with the number of adsorption cycles *n* (Figure 5a). However, the maximum of the Q band is red-shifted with respect to the maximum of the Q band for a diluted AB solution. This is a clear signature of AB aggregation in the film, an expected result for AB being confined in a

TABLE 1. Mass Density of the *In Silico* Produced Eumelanin, Compared with Published Experimental Data

source	mass density
our data, dry *in silico*	1.55 g/cm^3
our data, wet *in silico*	1.38 g/cm^3
J.M. Gallas[13]	1.4 g/cm^3
J.A. Swift[31]	1.54 g/cm^3
L. Zeise[29]	1.69 g/cm^3
J.H. Waite[30]	1.77 g/cm^3

TABLE 2. Young's Modulus of the *In Silico* Produced Eumelanin, Compared with Published Experimental Data

source	modulus (dry)	modulus (wet)
our data, *in silico*	5.0 ± 1.66 GPa	2.3 ± 1.28 GPa
B. Bhushan[32] (melanin granules)	7.02 ± 2.84 GPa	1.37 ± 1.18 GPa
J.H. Waite[30] (sepia)	6.75 ± 0.75 GPa	1.5 ± 0.25 GPa
J.H. Waite[30] (hydrolyzed jaw)	3.25 ± 0.5 GPa	1.75 ± 0.25 GPa

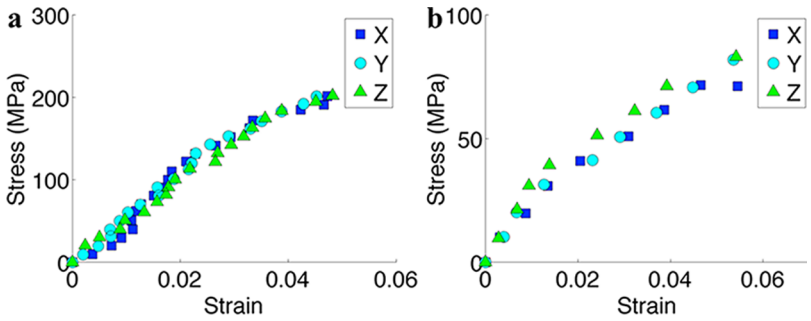

Figure 4. Young's modulus calculations of the *in silico* produced eumelanin: stress−strain curves for the aggregate made of 375 IMIM tetramers in the dry (a) and wet (b) eumelanin systems.

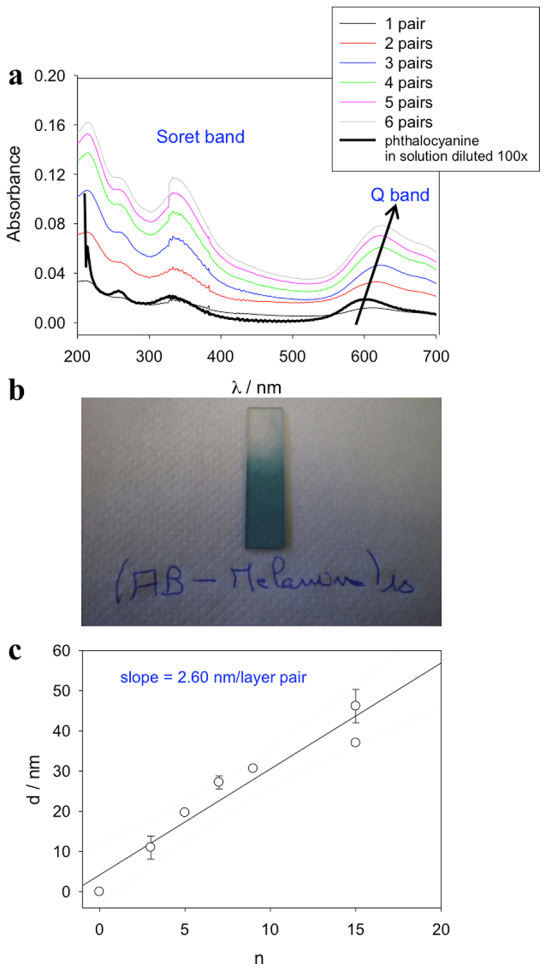

Figure 5. LBL assembly of AB and eumelanin. (a) UV−vis spectra of the (AB-melanin)$_n$ films for a different number of deposition cycles and UV−vis spectrum of a diluted AB solution used to deposit the films. The inset indicates the number of deposited layer pairs and the spectrum taken from a diluted AB solution. The arrow indicates the progressive red shift of the Q band when the number of eumelanin and AB deposition steps increases. (b) Photograph of a (AB-melanin)$_{10}$ film deposited on a quartz slide. (c) Evolution of the thickness of (AB-melanin)$_n$ films as calculated from spectroscopic ellipsometry data. Each point corresponds to an individual experiment. The full line corresponds to a linear regression to the data, and the dotted line corresponds to the limit of the 95% confidence interval. The error bars on each data point were calculated on the basis of the standard deviation of the film thickness calculated from five measurements along the main axis of the silicon slides used to deposit the films.

dense phase. The presence of eumelanin in such films is confirmed indirectly by the fact that no absorbance increase is observed after the first adsorption step of AB on a quartz slide when successive immersions in an AB solution are performed. In addition, the UV−vis spectra of the (AB-melanin)$_n$ films display a continuous decrease in absorbance as a function of increasing λ, a typical signature of the absorption spectrum of synthetic eumelanin (the spectrum of a eumelanin film is shown in Supporting Information Figure S5). The thickness increase of such films is linear with the number of deposition cycles n (Figure 5c), with a thickness

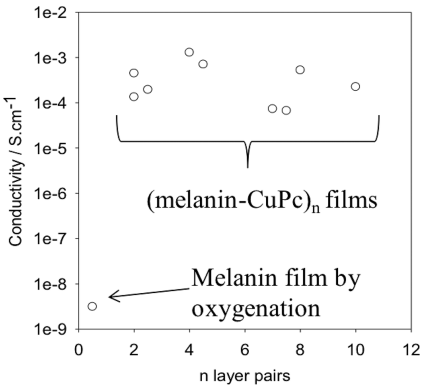

Figure 6. Electrical conductivity of a melanin film produced by oxygenation of a dopamine solution (2 g·L^{-1} in the presence of 50 mM Tris buffer at pH 8.5) and of (AB-melanin)$_n$ films.

increment of 2.6 nm per deposition cycle, and the films are continuous and relatively smooth (rms roughness of 4.6 nm for a film having a thickness of 13 nm as revealed by AFM, Supporting Information Figure S6).

The most interesting information is that those films display an electrical conductivity of $(4 \pm 3) \times 10^{-4}$ S·cm^{-1}, which is independent from their thickness and higher by 5 orders of magnitude than the conductivity of an eumelanin film (3×10^{-9} S·cm^{-1}) deposited directly from an aqueous dopamine solution (Figure 6).[36] Note that all of the conductivity measurements were performed on insulating quartz slides.

This means that the incorporation of the Cu(II) phthalocyanine, AB, in close proximity to the eumelanin particles allows us to produce a composite film displaying a satisfactory conductivity. The conductivity increase originates most probably from a close stacking of the almost planar AB with the surface of eumelanin grains as those displayed in Figure 3b−d. This assumption is confirmed by selected area electron diffraction (SAED) of melanin grains that have been put in contact with an AB solution at 10^{-4} M during 14 h and then intensively dialyzed against distilled water: the SAED pattern reveals indeed the presence of copper which is the elemental signature of AB (Supporting Information Figure S7). It might well be that AB totally covers the eumelanin particles during the layer-by-layer deposition process owing to strong $\pi-\pi$ interactions as well as electrostatic interactions, leading to a percolating network of conducting molecules surrounding insulating grains. This assumption remains to be confirmed in future investigations.

All of these data suggest that our model of eumelanin self-assembly is sufficient for an excellent prediction of the supramolecular structure of eumelanin (Figure 3a *vs* Figure 3b and Supporting Information Figure S3), its mass density (Table 1), and Young's modulus (Table 2). Note that our model limits the size of the oligomers to tetramers, whereas other models use eumelanin molecules made of the covalent association to 11 IQ

monomers stacking together *via* π stacking and produced *via* Diels–Alder reactions between IQ to describe the supramolecular structure of eumelanin.[31]

CONCLUSIONS

In this paper, we provided evidence for the hypothesis that eumelanin is obtained through the self-assembly of tetramers of 5,6-dihydroxyindole. We are able to predict the supramolecular structure of eumelanin through molecular dynamics simulations, which is in excellent agreement with TEM images of synthetic eumelanin. In addition, our model allows us to predict the mass density and Young's modulus of eumelanin in very good agreement with experimental values. The assumption that eumelanin is made of the self-assembly of tetramers of 5,6-dihydroxyindole, without covalent interactions between them, also allow us to design a composite layer-by-layer film between synthetic eumelanin particles and the cationic phthalocyanine AB. This composite exhibited an electrical conductivity 5 orders of magnitudes higher than that of pure eumelanin films. Our investigation shows that a better knowledge of the structure and self-assembly mechanism of eumelanin allows us to design new bioinspired composites with improved properties with respect to eumelanin itself.

MODELING AND EXPERIMENTAL METHODS

Generation of Tetramers of 5,6-Indolequinone. According to Kaxiras *et al.*,[20,21] there are 21 possible arrangements of four individual monomer units (HQ, IQ, MQ, and NQ) in an eumelanin model if we restrict the QI form (MQ and NQ) to one type. However, only eight of them that contain two or three QIs have large positive formation energy and are hence considered to be the dominant tetramers. In this paper, we use the most favorable structure among the eight dominant tetramers, the IMIM tetramer, which contains two IQ and two MQ monomers, as the eumelanin model for the simulations (Supporting Information Figure S1).

All-Atom Modeling and Equilibration. Full atomistic simulations are performed using the large-scale atomic/molecular massively parallel simulator (LAMMPS) with the consistent valence force field (CVFF) that includes parameters for the atom types and bonds of the eumelanin model. The CVFF is parametrized to reproduce peptide and protein properties and has been supplemented with several parameters for small organic molecules including dopamine.[37] Energy minimization using the conjugate gradient (CG) algorithm is performed before molecular dynamics simulations. The charge is taken into account in the simulations, and the total charge of an IMIM tetramer is zero (electroneutral). The integration time step is set as 0.5 fs, and the nonbonding interactions (the 12/6 Lennard-Jones interactions and Coulombic interactions) are computed using a cutoff for neighbor list at 12.0 Å.

In this paper, the building block of the large-scale systems includes three IMIM tetramers in the *X*, *Y*, and *Z* directions, respectively. The dry eumelanin system is built by replicating the initial system five times in each direction, and we therefore have 125 building blocks (375 IMIM tetramers, with 21 000 atoms). It is not clear in the eumelanin experiments what the water percentage of the wet eumelanin grains is. Here we assume that the mass of the hydration water is about one-half the mass of the eumelanin molecules. Therefore, in the wet eumelanin system, the building block includes three IMIM tetramers as the dry eumelanin system and an additional 48 water molecules around the tetramers. We created 125 building blocks (375 IMIM tetramers and 6000 water molecules, with a total of 39 000 atoms) in the wet eumelanin system using the replication command. The boundary conditions in the dry and wet eumelanin systems are both periodic. After energy minimization, the systems are simulated with NPT ensemble at a constant temperature of 1000 K and at a pressure of 1.013 bar for 2.0 ns, to ensure a sufficient exploration on the configurations of the obtained aggregates. The high temperature in the simulation allows the IMIM tetramers to reach the most stable configurations much faster than at the room temperature (300 K). However, we notice that there might be some empty holes in the systems after the previous NPT ensemble, and these empty holes will not disappear in the systems for a long time even if we cool the systems to 300 K. In order to remove these empty holes faster, the systems are then simulated with the NPT ensemble at a constant temperature of 300 K and a pressure of 1013 bar for another 2.0 ns. With the high pressure in the simulation, these empty holes will no longer be in the systems, and therefore, the mass density is nearly a constant in the entire system. Since we are interested in the mechanical properties of eumelanin at room temperature (300 K) and the standard atmospheric pressure, the systems are then simulated with the NPT ensemble at a constant temperature of 300 K and a pressure of 1.013 bar for another 2.0 ns.

Bond Length of the IQ Monomer Comparisons. The equilibrium bond lengths of the IQ monomer are calculated using the LAMMPS with the CVFF. The PDB file of the IQ monomer is adapted from the human metabolome database. Simon *et al.* calculated some bond lengths of the IQ monomer using DFT techniques,[38] and the results are very close to our calculations (see Supporting Information).

Analysis of the Orientations of IMIM Tetramers. The IMIM tetramer is a quasi-planar structure so that each such tetramer has its own orientation in an aggregate. Hence, we can define the orientation vector of each IMIM tetramer. We use the coordinates of the four nitrogen atoms of each IMIM tetramer to define the orientation vectors. First, we calculate two direction vectors: one is based on the two nitrogen atoms of the two IQ monomers, and the other one is based on the two nitrogen atoms of the two MQ monomers. The orientation vector of each IMIM tetramer is defined as the cross-product of the two direction vectors and normalized to be a unit vector (see Supporting Information Figure S9). This means that the orientation vector is orthogonal to the quasi-planar structure of each IMIM tetramer.

Analysis of the Stacking Mechanism of IMIM Tetramers and Formation of Secondary Structures. In order to decide whether two IMIM tetramers are stacking together or not, we use two criteria in our algorithm. First, we calculate the central position of each IMIM tetramer by averaging the coordinates of the four nitrogen atoms in each IMIM tetramer. Although the interlayer distance of two stacked IMIM tetramers is around 3.5–4.0 Å, the distance between the two central positions is usually larger than this range but smaller than 6.0 Å due to the π stacking. Hence, we define that, if two IMIM tetramers are considered to belong to the same secondary structure, the distance between the central positions must be smaller than 7.0 Å (see Supporting Information Figure S8). In addition to the distance requirement, we also use the orientation requirement. If the distance between two IMIM tetramers satisfies the distance requirement, we calculate the orientation vectors of these two IMIM tetramers. If the absolute value of the dot product of these two orientation vectors is larger than 0.95, which means that these two IMIM tetramers are almost parallel to each other, we determine that these two IMIM tetramers are stacking together in the same secondary structure.

Analysis of the Mass Density and Young's Modulus of Aggregates Produced from the Self-Assembly of IMIM Tetramers. After the three steps of simulations in the NPT ensemble (at 1000 K and 1.013 bar, 300 K and 1013 bar, and finally at 300 K and 1.013 bar), the equilibrium box sizes of the dry and wet eumelanin systems are 61.25 Å × 61.31 Å × 61.87 Å and 73.19 Å × 74.15 Å × 72.35 Å,

respectively. We then performed tensile tests to estimate the Young's modulus of eumelanin. The systems are simulated with the NPT ensemble at a constant temperature of 300 K; however, the tensile stress increases by 101.3 bar every 0.2 ns in one direction, and the pressure in the other two directions remains at 1.013 bar. During the simulations, we record the equilibrium box size of the systems, and therefore, we have the stress–strain curves for the Young's modulus calculations.

Synthesis of Eumelanin in Solution and Its Characterization. Dopamine (Sigma H8502, used without further purification) was dissolved at $2\,g\cdot L^{-1}$ (10^{-3} M) in a 50 mM Tris buffer ($C_4H_{11}NO_3$, Tris, ref 252859, Sigma-Aldrich) whose pH was adjusted to 8.5 with concentrated HCl. This solution was vigorously stirred (400 rpm with magnetic agitation) in an open-air reactor to allow for the oxidation of dopamine and the subsequent formation of eumelanin. The reaction was allowed to proceed for 24 h before degazing of the solution with N_2 and storage in a closed bottle.

Part of the obtained eumelanin solution was mixed with an equal volume of Tris buffer containing AB ($C_{56}H_{40}Cl_4CuN_{12}$, $M_W = 1086.36\ g\cdot mol^{-1}$, ref 335630, Sigma-Aldrich, Supporting Information Figure S4) at 2×10^{-4} M. This mixture was allowed to equilibrate for 24 h under magnetic stirring before dialysis against distilled water (Spectra Por membranes with molecular weight cut off of $10^4\ g\cdot mol^{-1}$) in order to eliminate the AB not bound to eumelanin. The solution to be dialyzed was 100 mL, and it was dialyzed three times against 900 mL of distilled water. The absence of AB in the dialysate was checked by means of UV–vis spectroscopy (Perkin-Elmer Lambda 35).

Conventional high-resolution transmission electron microscopy imaging and energy-dispersive X-ray spectroscoy (EDS) were conducted using a JEOL 2200F TEM/STEM at 100 kV acceleration voltages of the electrons to study the molecular organization of synthetic eumelanin. The composition of the eumelanin grains decorated with AB was investigated by EDS. All samples were deposited on a Ni TEM grid. More information can be found in Supporting Information Figures S3 and S7.

Synthesis of New Conductive Films from Melanin Particles and AB Phthalocyanines Using the LBL Method. The quartz slides (4 cm × 1 cm × 0.1 cm, Thuet, Blodelsheim, France) and the (111) silicon slides (P-doped, Siltronix, Archamps, France) were cleaned before each experiment. The quartz slides and the silicon wafers were rinsed with ethanol, dried under a stream of nitrogen, and immersed in a freshly prepared piranha solution (1:3 v/v of a 30% H_2O_2 solution and 98% H_2SO_4) for 30 min and finally extensively rinsed with Milli-Q water. Each slide was cleaned just before the deposition of the $(AB\text{-melanin})_n$ films. The same cleaning method applies for the quartz slides used for the deposition of a eumelanin film from an oxygenated dopamine solution. *Caution: The piranha solution is extremely corrosive and should be handled with extreme precaution.*

The adsorption substrates were then dipped manually in an AB solution for 1 min, in two beakers containing Tris buffer, in the eumelanin solution, and again in two beakers containing Tris buffer. The deposition of AB followed by the deposition of eumelanin constitutes one deposition cycle which was reiterated n times to yield $(AB\text{-eumelanin})_n$ films. The absorbance of these coatings deposited on quartz slides was followed by means of UV–vis spectroscopy (using an uncoated quartz slide as a reference) using a double-beam spectrophotometer (Perkin-Elmer Lambda 35). The films deposited on quartz slides were also used for four-point conductivity measurements (Ecopia HMS-3000) applying a magnetic field of 0.54 T for the Hall effect measurements. The thickness of the films deposited on silicon slides was calculated from ellipsometry measurements. The film thickness was calculated from spectroscopic ellipsometry measurements using an AUTO SE spectroscopic ellipsometer (Horiba, France) working in the wavelength range between 450 and 1000 nm. The ellipsometric output, namely, the $\Delta(\lambda)$ and $\psi(\lambda)$ angles, was used to calculate the film thickness and the real and imaginary part of its refractive index. For that aim, we used a three-layer model, in which the first layer was the semi-infinite Si, the second layer was a 2 nm thick SiO_2 layer, and the third layer was made of the $(AB\text{-melanin})_n$ film considered to be homogeneous and isotropic. The validity of this assumption will be discussed by comparing the film thickness calculated from the ellipsometric data to the thickness value measured by atomic force microscopy. The thickness and refractive index values correspond to the average (±1 SD) over three measurements on regularly spaced locations along the major axis of the silicon wafer. The LBL film was fitted with a dispersion law corresponding to that of a semiconductor with a nonzero value for the imaginary part of the refractive index. Note that the simultaneous use of AFM and ellipsometry to determine the thickness of the films avoids overinterpreting ellipsometry data which rely on the use of an optical model to calculate the refractive index and the thickness of the film. AFM provides accurate and model independent film thickness provided that the roughness of the coating is small and that the piezoscanner is well-calibrated.

The thickness was assumed to be the same on silicon (covered with about 20 Å of spontaneously grown silicon oxide) and on quartz and was taken into account for the calculation of the film's conductivity from the measured resistance. As reference of pure eumelanin films for the electrical conductivity measurements, we produced a eumelanin film of about 45 nm in thickness on a cleaned quartz slide according to the method proposed by Messersmith *et al.*[36]

Conflict of Interest: The authors declare no competing financial interest.

Acknowledgment. C.T.C. and M.J.B. are supported by CRP Henri Tudor in the framework of the BioNanotechnology project.

Supporting Information Available: Molecular structure of the IMIM tetramer, components of the orientation vectors of the IMIM tetramers, bright field TEM micrographs of eumelanin grains on Ni grids, structure of the cationic Cu(II) tetrapyridinophthalocyanine used for the LBL deposition, UV–vis spectrum of an eumelanin film deposited on quartz slides, AFM topography in the dry state of an $(AB\text{-eumelanin})_5$ film, SAED of an AB-eumelanin composite, bond length of IQ monomer comparisons, and additional methodological details. This material is available free of charge *via* the Internet at http://pubs.acs.org.

REFERENCES AND NOTES

1. Meredith, P.; Sarna, T. The Physical and Chemical Properties of Eumelanin. *Pigm. Cell Res.* **2006**, *19*, 572–594.
2. Bothma, J. P.; de Boor, J.; Divakar, U.; Schwenn, P. E.; Meredith, P. Device-Quality Electrically Conducting Melanin Thin Films. *Adv. Mater.* **2008**, *20*, 3539–3542.
3. Ball, V.; Del Frari, D.; Michel, M.; Buehler, M.; Toniazzo, V.; Singh, M.; Gracio, J.; Ruch, D. Deposition Mechanism and Properties of Thin Polydopamine Films for High Added Value Applications in Surface Science at the Nanoscale. *BioNanoScience* **2012**, *2*, 16–34.
4. Peles, D. N.; Hong, L.; Hu, D.-N.; Ito, S.; Nemanich, R. J.; Simon, J. D. Human Iridal Stroma Melanosomes of Varying Pheomelanin Contents Possess a Common Eumelanic Outer Surface. *J. Phys. Chem. B* **2009**, *113*, 11346–11351.
5. Jastrzebska, M.; Kocot, A.; Vij, J. K.; Zalewska-Rejdak, J.; Witecki, T. Dielectric Studies on Charge Hopping in Melanin Polymer. *J. Mol. Struct.* **2002**, *606*, 205–210.
6. Liu, Y.; Hong, L.; Kempf, V. R.; Wakamatsu, K.; Ito, S.; Simon, J. D. Ion-Exchange and Adsorption of Fe(III) by Sepia Melanin. *Pigm. Cell Res.* **2004**, *17*, 262–269.
7. Kollias, N.; Sayre, R. M.; Zeise, L.; Chedekel, M. R. New Trends in Photobiology: Photoprotection by Melanin. *J. Photochem. Photobiol., B* **1991**, *9*, 135–160.
8. Clancy, C. M. R.; Nofsinger, J. B.; Hanks, R. K.; Simon, J. D. A Hierarchical Self-Assembly of Eumelanin. *J. Phys. Chem. B* **2000**, *104*, 7871–7873.
9. Pezzella, A.; d'Ischia, M.; Napolitano, A.; Palumbo, A.; Prota, G. An Integrated Approach to the Structure of Sepia Melanin. Evidence for a High Proportion of Degraded 5,6-Dihydroxyindole-2-carboxylic Acid Units in the Pigment Backbone. *Tetrahedron* **1997**, *53*, 8281–8286.

10. Cheng, J. I. N.; Moss, S. C.; Eisner, M.; Zschack, P. X-ray Characterization of Melanins—I. *Pigm. Cell Res.* **1994**, *7*, 255–262.
11. Cheng, J. I. N.; Moss, S. C.; Eisner, M. X-ray Characterization of Melanins—II. *Pigm. Cell Res.* **1994**, *7*, 263–273.
12. Zajac, G. W.; Gallas, J. M.; Cheng, J.; Eisner, M.; Moss, S. C.; Alvarado-Swaisgood, A. E. The Fundamental Unit of Synthetic Melanin: A Verification by Tunneling Microscopy of X-ray Scattering Results. *Biochim. Biophys. Acta* **1994**, *1199*, 271–278.
13. Gallas, J. M.; Littrell, K. C.; Seifert, S.; Zajac, G. W.; Thiyagarajan, P. Solution Structure of Copper Ion-Induced Molecular Aggregates of Tyrosine Melanin. *Biophys. J.* **1999**, *77*, 1135–1142.
14. Clancy, C. M. R.; Simon, J. D. Ultrastructural Organization of Eumelanin from Sepia Officinalis Measured by Atomic Force Microscopy. *Biochemistry* **2001**, *40*, 13353–13360.
15. Dreyer, D. R.; Miller, D. J.; Freeman, B. D.; Paul, D. R.; Bielawski, C. W. Elucidating the Structure of Poly(dopamine). *Langmuir* **2012**, *28*, 6428–6435.
16. Della Vecchia, N. F.; Avolio, R.; Alfè, M.; Errico, M. E.; Napolitano, A.; d'Ischia, M. Building-Block Diversity in Polydopamine Underpins a Multifunctional Eumelanin-Type Platform Tunable through a Quinone Control Point. *Adv. Funct. Mater.* **2012**, 10.1002/adfm.201202127.
17. Napolitano, A.; Pezzella, A.; Prota, G.; Seraglia, R.; Traldi, P. Structural Analysis of Synthetic Melanins from 5,6-Dihydroxyindole by Matrix-Assisted Laser Desorption/Ionization Mass Spectrometry. *Rapid Commun. Mass Spectrom.* **1996**, *10*, 468–472.
18. Stark, K. B.; Gallas, J. M.; Zajac, G. W.; Eisner, M.; Golab, J. T. Spectroscopic Study and Simulation from Recent Structural Models for Eumelanin: II. Oligomers. *J. Phys. Chem. B* **2003**, *107*, 11558–11562.
19. Stark, K. B.; Gallas, J. M.; Zajac, G. W.; Eisner, M.; Golab, J. T. Spectroscopic Study and Simulation from Recent Structural Models for Eumelanin: I. Monomer, Dimers. *J. Phys. Chem. B* **2003**, *107*, 3061–3067.
20. Kaxiras, E.; Tsolakidis, A.; Zonios, G.; Meng, S. Structural Model of Eumelanin. *Phys. Rev. Lett.* **2006**, *97*, 218102.
21. Meng, S.; Kaxiras, E. Theoretical Models of Eumelanin Protomolecules and Their Optical Properties. *Biophys. J.* **2008**, *94*, 2095–2105.
22. Bridelli, M. G. Self-Assembly of Melanin Studied by Laser Light Scattering. *Biophys. Chem.* **1998**, *73*, 227–239.
23. Miyasaka, Y.; Nakamura, A.; Temmyo, J. Graphite Thin Films Consisting of Nanograins of Multilayer Graphene on Sapphire Substrates Directly Grown by Alcohol Chemical Vapor Deposition. *Jpn. J. Appl. Phys.* **2011**, *50*, 04DH12.
24. Park, J. H.; Aluru, N. R. Self-Assembly of Graphenes. *Surf. Sci.* **2011**, *605*, 1616–1620.
25. Watt, A. A. R.; Bothma, J. P.; Meredith, P. The Supramolecular Structure of Melanin. *Soft Matter* **2009**, *5*, 3754–3760.
26. Herlinger, E.; Jameson, R. F.; Linert, W. Spontaneous Autoxidation of Dopamine. *J. Chem. Soc., Perkin Trans. 2* **1995**, 259–263.
27. Raper, H. S. The Tyrosinase-Tyrosine Reaction. VI. Production from Tyrosine of 5:6-Dihydroxyindole and 5:6-Dihydroxyindole-2-carboxylic Acid—The Precursors of Melanin. *Biochem. J.* **1927**, *21*, 89–96.
28. Bernsmann, F.; Ponche, A.; Ringwald, C.; Hemmerlé, J.; Raya, J.; Bechinger, B.; Voegel, J.-C.; Schaaf, P.; Ball, V. Characterization of Dopamine-Melanin Growth on Silicon Oxide. *J. Phys. Chem. C* **2009**, *113*, 8234–8242.
29. Zeise, L.; Addison, R. B.; Chedekel, M. R. Bio-Analytical Studies of Eumelanins. I. Characterization of Melanin the Particle. *Pigm. Cell Res.* **1992**, *2*, 48–53.
30. Moses, D. N.; Mattoni, M. A.; Slack, N. L.; Waite, J. H.; Zok, F. W. Role of Melanin in Mechanical Properties of Glycera Jaws. *Acta Biomater.* **2006**, *2*, 521–530.
31. Swift, J. A. Speculations on the Molecular Structure of Eumelanin. *Int. J. Cosmet. Sci.* **2009**, *31*, 143–150.
32. Bhushan, B. *Springer Handbook of Nanotechnology*, 2nd ed.; Springer: Berlin, 2007.
33. Hatton, R. A.; Blanchard, N. P.; Stolojan, V.; Miller, A. J.; Silva, S. R. P. Nanostructured Copper Phthalocyanine-Sensitized Multiwall Carbon Nanotube Films. *Langmuir* **2007**, *23*, 6424–6430.
34. Ball, V. Impedance Spectroscopy and Zeta Potential Titration of Dopa-Melanin Films Produced by Oxidation of Dopamine. *Colloids Surf., A* **2010**, *363*, 92–97.
35. Decher, G. Fuzzy Nanoassemblies: Toward Layered Polymeric Multicomposites. *Science* **1997**, *277*, 1232–1237.
36. Lee, H.; Dellatore, S. M.; Miller, W. M.; Messersmith, P. B. Mussel-Inspired Surface Chemistry for Multifunctional Coatings. *Science* **2007**, *318*, 426–430.
37. Gaedt, K.; Höltje, H.-D. Consistent Valence Force-Field Parameterization of Bond Lengths and Angles with Quantum Chemical *Ab Initio* Methods Applied to Some Heterocyclic Dopamine D3-Receptor Agonists. *J. Comput. Chem.* **1998**, *19*, 935–946.
38. Il'ichev, Y. V.; Simon, J. D. Building Blocks of Eumelanin: Relative Stability and Excitation Energies of Tautomers of 5,6-Dihydroxyindole and 5,6-Indolequinone. *J. Phys. Chem. B* **2003**, *107*, 7162–7171.